

ARTICLE TYPE

Evidence for the spin-kick alignment of pulsars from the statistics of their magnetic inclinations

A. Biryukov^{1,2,3} and G. Beskin⁴¹The Raymond and Beverly Sackler School of Physics and Astronomy, Tel Aviv University, Tel Aviv, 6997801, Israel²Sternberg Astronomical Institute, Lomonosov Moscow State University, 13 Universitetsky pr., Moscow, 119234, Russia³Institute of Physics, Kazan Federal University, 18 Kremlyovskaya st., Kazan, 420008, Russia⁴Special Astrophysical Observatory, Nijniy Arkhyz, Karachaevo-Cherkessia, 369167, Russia

Author for correspondence: A. Biryukov, Email: ant.biryukov@gmail.com.

Abstract

Isolated neutron stars are thought to receive a natal kick velocity at birth nearly aligned with their spin axis. Direct observational confirmation of this alignment has been limited to a single source in a supernova remnant (PSR J0538+2817) whose three-dimensional velocity has been well-constrained. Pulsar polarisation statistical properties indicate the presence of a spin-kick correlation, but aligned and orthogonal cases remain plausible. However, if the three-dimensional velocities of radiopulsars are indeed predominantly aligned with their spin axes, a systematic difference in the observed transverse velocities of pulsars with small and large magnetic obliquities would be expected. In particular, due to projection effects, weakly oblique rotators should show systematically smaller and less scattered transverse velocities. In contrast, transverse velocities of pulsars with large obliquities should be close to their actual three-dimensional velocities. This study analyzed samples of 13 weakly and 25 strongly oblique pulsars with known distances and proper motions. We find their peculiar velocities being distributed differently with the statistical confidence of 0.007 and 0.016 according to Anderson–Darling and Kolmogorov–Smirnov tests, respectively. We performed a detailed population synthesis of the isolated pulsars, considering the evolution of their viewing geometry in both isotropic and spin-aligned kick scenarios. The observed split in the transverse velocity distributions and its amplitude are consistent with the spin-aligned kick model but not the isotropic case. At the same time, an orthogonal kick predicts a similar effect but of the opposite sign. This provides robust support for pulsar spin-kick alignment based on their statistics and independent of their polarization properties.

Keywords: pulsars: general, methods: statistic, pulsars: velocities**1. Introduction**

The peculiar velocities of isolated radiopulsars with respect to the galactic environment are $\sim 200 - 500 \text{ km s}^{-1}$ (e.g. Igoshev 2020) which is markedly faster than $\sim 15 - 40 \text{ km s}^{-1}$ observed for their high-mass progenitors (e.g. Tetzlaff, Neuhauser, and Hohle 2011; Carretero-Castrillo, Ribó, and Paredes 2023). This indicates that neutron stars undergo a substantial natal kick during their formation in supernova explosions. Unfortunately, the absence of observational techniques to determine full three-dimensional velocities of neutron stars^a has impeded the firm establishment of the statistical properties of their galactic motion. Therefore, the details of the distribution of pulsar kicks remain somewhat uncertain. Thus, some researchers advocate for a broad unimodal velocity distribution (Faucher-Giguère and Kaspi 2006; Hobbs et al. 2005; Chatterjee et al. 2009), while others identify two components exhibiting typical dispersions of ~ 100 and $\sim 500 \text{ km s}^{-1}$, respectively (Cordes and Chernoff 1998; Arzoumanian, Chernoff, and Cordes 2002; Verbunt, Igoshev, and Cator 2017).

At the same time, neutron stars' velocities are thought to be related to their rapid spin-up at birth since both processes could result from the interaction between the newborn star

and supernova ejecta (e.g. Wang, Lai, and Han 2007; Janka 2017; Janka, Wongwathanarat, and Kramer 2022; Coleman and Burrows 2022). Therefore, it makes sense to expect a correlation between the pulsar spin axis and velocity directions. At least for the peculiar part of the velocity of objects younger than ~ 10 Myr, as such correlation erodes at the galactic dynamical timescales (Mandel and Igoshev 2023).

Studies of pulsar radio emission have shown that their apparent transverse velocities are not isotropically distributed relative to their spin axes, indicating a strong spin-velocity correlation (Simon Johnston et al. 2005; Wang, Lai, and Han 2006; Noutsos et al. 2012; Noutsos et al. 2013). This analysis was based on the Rotating Vector Model (RVM) applied to the pulsar linear polarization signal. This model assumes that the polarization position angle follows the projection of a rotating dipole field onto the viewing plane (Radhakrishnan and Cooke 1969; Lyutikov 2016). However, two types of degeneration are essential for such an approach. Firstly, two orthogonal polarization modes are possible for electromagnetic waves propagating through the magnetic field. These X- and O- (extraordinary and ordinary, respectively) modes can appear in observations of a single pulsar and can not be distinguished (Stinebring et al. 1984; Gangadhara 1997; Wang, Wang, and Han 2014). Secondly, RVM is insensitive to the spin direction of a radiopulsar: a clockwise rotator shows the same

a. See, however, the discussion in Sect. 2.5.3 by Edwards, Hobbs, and Manchester 2006

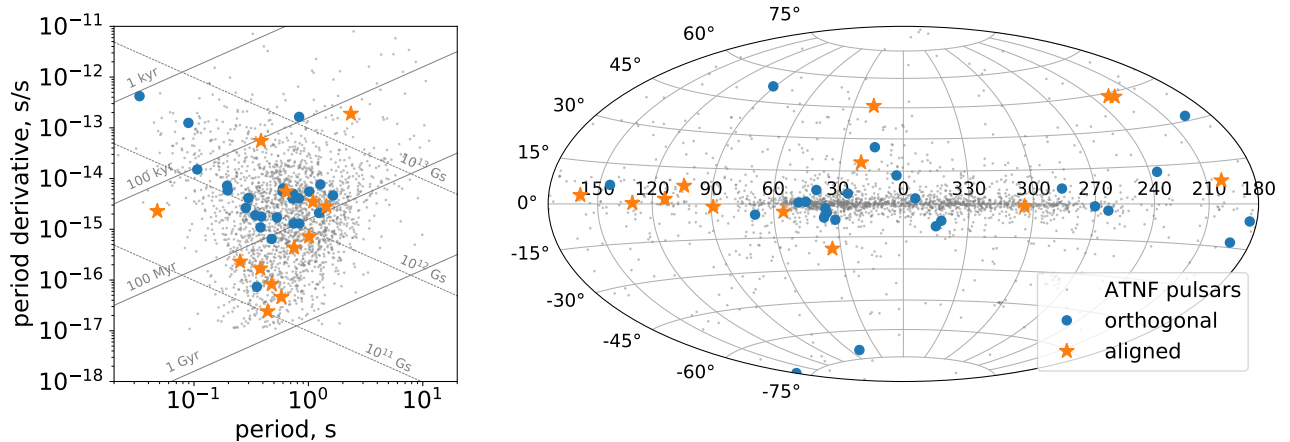


Figure 1. Pulsars under consideration. Left plot: classical $P - \dot{P}$ pulsar diagram. Orange stars show aligned rotators (with small magnetic angles). Blue circles show orthogonal ones (with large magnetic angles). Grey dots represent classical (non-recycled) isolated pulsars listed in the ATNF catalogue. Right plot: The same pulsars are plotted in the Galactic sky coordinates.

polarization behaviour as a counter-clockwise one. In combination, these degeneracies prevent the decision of whether pulsar velocities are aligned with their spins or perpendicular to them. Both scenarios remain possible.

Nevertheless, Yao *et al.* 2021 have recently presented the first clear detection of three-dimensional spin-velocity alignment in PSR J0538+2817. However, this is the only such evidence obtained so far. Therefore, alternative observational verification, which involves statistics of a subset of objects and which is independent of polarization, is relevant.

This work presents a method to test spin-velocity alignment in isolated radiopulsars based on geometric considerations. If pulsars' spins align with their velocities, then the transverse components of the latter for objects with different magnetic angles must differ. Magnetically aligned pulsars (with small spin-magnetic axis angles) move nearly along the line of sight, resulting in small, weakly scattered transverse velocities. In contrast, magnetically orthogonal pulsars move perpendicular to the line of sight, so their transverse velocities are close to the full 3D velocities. As a result, one would expect different transverse velocity distributions for nearly aligned and orthogonal pulsars.

We test this idea using existing data on magnetic inclinations, proper motions, and distances of isolated radiopulsars. Additionally, we perform detailed population synthesis to verify that the observed difference in the velocity distribution is consistent with the properties of a realistic population and can be detected in observations.

The paper is organized as follows. In Section 2, we compare transverse velocities of radiopulsars with different magnetic obliquities. Section 3 describes the population synthesis of these objects, with results presented in Section 4. A brief discussion and conclusions are provided in Section 5. Appendix 1 contains the table with precise details of the pulsar subset under investigation and figures that show the expanded results of the undertaken population synthesis.

2. Pulsars' velocities distributions

2.1 Magnetically orthogonal and aligned pulsars

To compare the transverse velocities of magnetically aligned and orthogonal pulsars, one has to create representative subsets of observed sources for both alignment types. In our previous work Biryukov and Beskin 2023, we compiled a catalogue of 77 isolated radiopulsars identified in the literature as having extreme magnetic inclination angles: either small (α near 0) or large (α near 90 degrees). The most reliable method for estimating α involves fitting the rotating vector model (RVM) to the pulsar's linear polarization signal. This model assumes that the observed swing of the polarisation position angle (PA) across the pulsar phase corresponds to the projection of a rotating dipole magnetic field onto the observer's plane of view Radhakrishnan and Cooke 1969; Lyutikov 2016. However, achieving high precision in estimating α often proves challenging, primarily due to the low signal-to-noise ratio in the outer "wings" of the average pulse profile. But polarization data carry the most information about the magnetic inclination angle in this part of the pulse Wang *et al.* 2023; S. Johnston *et al.* 2023. Therefore, an accurate magnetic angle for a particular pulsar is usually unknown.

However, some pulsar emission properties could provide valuable information for distinguishing between weakly and strongly oblique rotators. Without a precise estimation of the angle. These include average pulse widths, distinguishable core and cone emission components, existing of the interpulse, and qualitatively different polarization behaviour in both the main pulse and interpulse. Many authors have utilized these properties to classify pulsars into two categories (Lyne and Manchester 1988; Joanna M. Rankin 1990; J. M. Rankin 1993b; Maciesiak, Gil, and Ribeiro 2011; Keith *et al.* 2010; Malov and Nikitina 2013; Johnston and Kramer 2019). The list of 77 pulsars mentioned above was based on these classification arguments. For the present study, we extracted a subset from it, retaining only objects with determined full proper motions and distances. We found 13 nearly aligned and 25 nearly or-

thogonal rotators that meet these conditions. In Figure 1, these pulsars are plotted on the classical $P - \dot{P}$ diagram and within the galactic coordinates, alongside other single, non-recycled pulsars from the ATNF database (Manchester et al. 2005)^b. Despite the limited sample size, the selected pulsars provide a representative cross-section of the overall pulsar population. Details of the selected pulsars are presented in Table 2 in Appendix 1. Parameters of these objects were also taken from the ATNF. Half of the distances were estimated from dispersion measures, while the other 19 objects have independently determined parallaxes.

2.2 Pulsars' peculiar velocities

Let's consider the motion of pulsars relative to the galactic inertial reference frame (x, y, z) , with its origin in the Solar System Barycentre. Let the x -axis be directed towards the galactic centre; the y -axis is along the galactic rotation, while the z -axis points to the north galactic pole. If l and b are the pulsar's galactic coordinates, and μ_l and μ_b are the corresponding proper motions, with d being the distance to it, then the apparent pulsar's transverse velocity vector is

$$\mathbf{v}_t = kd\mu_l \begin{pmatrix} -\sin l \cos b \\ \cos l \cos b \\ 0 \end{pmatrix} + kd\mu_b \begin{pmatrix} -\cos l \sin b \\ -\sin l \sin b \\ \cos b \end{pmatrix}, \quad (1)$$

where $k \approx 4.74 \text{ km s}^{-1}/(\text{pc arcsec yr}^{-1})$. Physically, this velocity comprises the galactic motion of the Sun, the circular velocity of a pulsar's local standard of rest (LSR) in the Galaxy, and the peculiar velocity $\mathbf{v}_{pec,t}$ relative to the LSR. We assume that only the latter component generally contains information about the kick that a pulsar received after a supernova explosion. And therefore, it relates to the kick-velocity correlation. Although this correlation spreads out over a pulsar's lifetime (Mandel and Igoshev 2023), it still makes sense for relatively young objects that have not yet crossed their death line (see also section 4.1 below).

In this work, we, therefore, focus on the statistics of the projection of the pulsar's peculiar velocity onto the viewing plane associated with the star:

$$\mathbf{v}_{pec,t} = \mathbf{v}_t + \mathbf{v}_{\odot,t} - \mathbf{v}_{circ,t}, \quad (2)$$

where

$$\mathbf{v}_{\odot,t} = \mathbf{v}_{\odot} - (\mathbf{v}_{\odot} \cdot \mathbf{n})\mathbf{n} \quad (3)$$

is the projection of the Solar System's Barycenter galactic velocity. Unit vector \mathbf{n} is directed towards the pulsar:

$$\mathbf{n} = \begin{pmatrix} \cos l \cos b \\ \sin l \cos b \\ \sin b \end{pmatrix}. \quad (4)$$

In our calculations, we adopt an approximate value

$$\mathbf{v}_{\odot} = (10, 235, 7.5) \text{ km s}^{-1}, \quad (5)$$

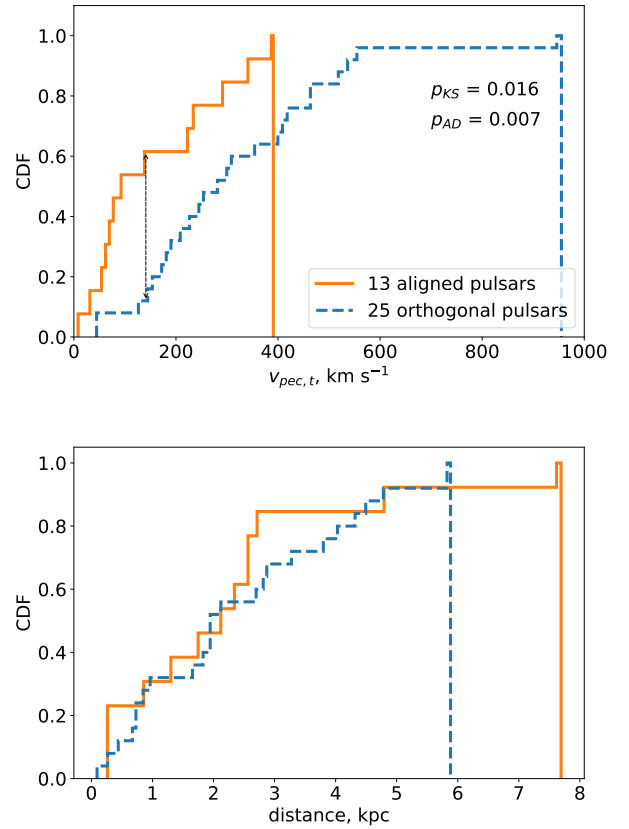


Figure 2. Top plot: Cumulative distributions of the absolute values of the transverse peculiar velocities for both types of pulsars. The solid orange line represents weakly oblique (“aligned”) rotators, while the dashed blue line represents strongly oblique (“orthogonal”) rotators. There are 13 aligned and 25 orthogonal pulsars used, whose parameters are listed in Table 2 in Appendix 1. Two distributions are different: orthogonal rotators show systematically larger and highly scattered velocities. The Kolmogorov-Smirnov two-sample test rejects the hypothesis that both subsets represent the same parent distribution at the $p_{KS} = 0.016$ confidence, and the Anderson-Darling test gives $p_{AD} = 0.007$. The divergence between two distributions can be interpreted as an imprint of the pulsar spin-kick alignment. In particular, magnetically aligned pulsars tend to move along the line of sight, while orthogonal rotators move perpendicular to it. Bottom plot: Cumulative distributions of estimated distances for both types of pulsars. Their similarity suggests that the difference detected in the top plot is not due to systematic differences in distance measures.

which is well consistent with recent estimations (Schönrich, Binney, and Dehnen 2010; Disberg, Gaspari, and Levan 2024). We do not need to know this particular velocity with high accuracy due to the uncertainties in estimating the distance of pulsars from their dispersion measures. Moreover, for the circular velocity $\mathbf{v}_{circ,t}$ we also use a simplified (fully analytic) but reasonable model of the 3-component gravitational potential $\phi(R, z)$ in the form offered by Carlberg and Innanen 1987 and modified by Kuijken and Gilmore 1989. Calculating

$$\mathbf{v}_{circ}(R) = \sqrt{R \cdot \nabla \phi(R, 0)} \begin{pmatrix} \gamma \\ -x + R_{\odot} \\ 0 \end{pmatrix}, \quad (6)$$

^b v2.0.0, available at <https://www.atnf.csiro.au/research/pulsar/psrv2.0/>. We assume it to be aligned with the galactic plane and depend-

ing only on cylindrical radius $R = \sqrt{x^2 + y^2}$ and galactocentric distance of the Sun $R_\odot = 8.5$ kpc. The latter value is consistent with the adopted gravitational potential.

In the top plot of Figure 2, we show the cumulative distributions of the absolute values $|v_{pec,t}|$ for both types of pulsars. The difference between these two distributions is clear: orthogonal rotators (shown with the blue dashed line) have systematically larger and highly scattered velocities. This is precisely what one would expect in the case of spin-kick alignment. The Kolmogorov-Smirnov two-sample test rejects the hypothesis that both subsets represent the same parent distribution at the $p_{KS} = 0.016$ confidence, and the Anderson-Darling test detects an even more significant difference: $p_{AD} = 0.007$. At the same time, this difference is not a result of the systematics of the distance estimates: the distributions of the distances for both groups are almost the same, as shown in the lower plot of Figure 2.

These distributions can be understood assuming that aligned pulsars tend to move along the line of sight and thus show little dispersion in their transverse velocities. This is entirely consistent with the spin-kick alignment hypothesis. However, we cannot determine whether the kick is in the same direction as or opposite to the pulsar’s spin axis. This is the first direct kinematic and simultaneously population-based evidence for the pulsar spin-kick alignment.

We have performed a detailed population synthesis of radiopulsars to provide a robust theoretical argument that this difference is indeed expected and detectable. The fundamental difficulty here is to accurately account for the selection bias in the estimates of the transverse velocities. As these quantities in our subset have been measured with different instruments and techniques, we only pretend to justify the described distribution splitting effect’s existence and approximate its amplitude.

3. Population synthesis

For reasons of simplicity, in our work, we generally reproduce the well-established algorithm initially described by Faucher-Giguère and Kaspi 2006 (hereinafter FK06) with some modifications relevant to the aim of the analysis. In this section, we describe our model and computational setup in detail.

3.1 Pulsar initial galactic positions

Coordinates and velocities of synthetic pulsars were considered within the galactocentric cartesian right-handed reference frame with the observer shifted from the centre for $R_\odot = 8.5$ kpc and located within the equatorial plane. Following FK06, we simulate the positions of newborn pulsars along the four spiral arms established by Georgelin and Georgelin 1976 and quantified by Wainscoat et al. 1992. All birth locations were then smoothed relative to spiral arms centroids, as described in FK06 as well.

However, the surface density of newborn pulsars’ was modelled in a slightly different way as

$$p(R) = A \left(\frac{R}{R_\odot} \right)^4 \times \exp \left(-6.8 \cdot \frac{R}{R_\odot} \right), \quad (7)$$

where R is the galactocentric cylindrical radius and $A \approx 71.3$ is a normalization constant (Yusifov and Küçük 2004). This distribution describes the localization of young OB-type stars that are believed to be neutron star progenitors. In FK06, another distribution was adopted for the same task. Specifically, $p(R)$ of *evolved* pulsars has been used, which is slightly different from (7) and which was also found by Yusifov and Küçük 2004. However, expression (7) seems more physically motivated and, as demonstrated below, successfully reproduces observed pulsar statistics.

For pulsar birth places along the galactic z -axis (vertical), the double-sided exponential distribution with $\langle z_0 \rangle = 50$ pc has been used.

3.2 Pulsar initial velocities

Initial velocities of synthetic pulsars were calculated as a vector sum of the progenitor’s circular velocity (6) and isotropic kick velocity \mathbf{v}_{kick} . The absolute value of the latter was based on the double-sided exponential distribution

$$p(v_{1D}) = \frac{1}{\langle v_{1D} \rangle} \exp \left(-\frac{|v_{1D}|}{\langle v_{1D} \rangle} \right) \quad (8)$$

with $\langle v_{1D} \rangle = 180$ km s⁻¹ as was found by FK06. According to this, the average full 3-dimensional velocity of newborn pulsars is $\langle v_{kick,3D} \rangle = 380$ km s⁻¹.

3.3 Spin-kick alignment

Two scenarios of spin-kick relationship were investigated: the isotropic and the statistically aligned one.

For every synthetic pulsar, a unit vector \mathbf{w} , representing the orientation of its spin axis, has been generated. In the case of *isotropic kick*, vector \mathbf{w} has been modelled independently on \mathbf{v}_{kick} . In turn, in the case of *aligned kick*, it was generated so that the angle between \mathbf{v}_{kick} and \mathbf{w} follow a zero-centred normal distribution with standard deviation $\sigma_{kick} = 15^\circ$. This value is consistent with empirical estimations by Noutsos et al. 2012. In particular, such σ_{kick} correspond to the reasonably small value that allows to reproduce the distribution of the angle Ψ between the pulsar velocity and spin axes projections onto the viewing plane (see also Section 4.1).

3.4 Pulsar physical parameters and their evolution

Pulsar ages

Ages of synthetic pulsars were generated uniformly within the interval from 0 to 1.2 Gyr, which corresponds to the constant birthrate of galactic pulsars over the last 1.2 Gyrs. The upper bound of this interval is determined by the longest pulsar lifetime within the adopted spin-down and deathline models (see below). The equation of motion of synthetic pulsars is $\ddot{\mathbf{r}} = -\nabla\phi(\mathbf{r})$ has been solved numerically until the prescribed pulsar age. During these calculations, we control a pulsar’s total (kinetic plus potential) energy and reject the result if it diverges for more than 1 per cent over the pulsar’s lifetime.

Spin-down model

In contrast to FK06, we adopt a more realistic pulsar spin-down model derived within the MHD and PIC simulations (Spitkovsky 2006; Philippov, Tchekhovskoy, and Li 2014). Thus, the evolution of pulsar spin period $P(t)$ was described as

$$P(t) \cdot \frac{dP(t)}{dt} = kB^2 \left[1 + 1.4 \sin^2 \alpha(t) \right]. \quad (9)$$

Here B is a constant surface (dipolar) magnetic field, $\alpha(t)$ is the variable angle between the pulsar magnetic and spin axes while $k = 4\pi^2 R_{\text{NS}}^6 / I c^3 = 1.75 \times 10^{-39} \text{ sec/Gs}^2$. Neutron star radius R_{NS} and moment of inertia I in this constant were taken for a $1.5M_{\odot}$ mass star assuming the WFF2 equation of state (Wiringa, Fiks, and Fabrocini 1988). The evolution of the magnetic angle $\alpha(t)$ was modelled in a consistent way as

$$P(t)^2 \cdot \frac{d\alpha(t)}{dt} = -4\pi^2 kB \sin \alpha(t) \cdot \cos \alpha(t). \quad (10)$$

Distribution of pulsar initial periods $P_0 = P(0)$ was assumed to be normal with average $\langle P_0 \rangle$ and standard deviation $\sigma[P_0]$, where $\langle P_0 \rangle$ and $\sigma[P_0]$ are the free parameters of our model whose values were estimated within the optimization procedure. The same is true for the distribution of magnetic fields (described via $\langle \log B \rangle$ and $\sigma[\log B]$).

At the same time, Initial values for the magnetic angle $\alpha_0 \in 0..90^\circ$ were taken from the isotropic distribution so that

$$p(\alpha_0) = \frac{1}{2} \sin \alpha_0. \quad (11)$$

Radio luminosity

Pulsar pseudo-luminosity^c at the frequency 1.4GHz was modelled in a way similar to that offered by Gullón et al. 2014:

$$L_{1.4\text{GHz}} = L_0 \cdot 10^{L_{\text{corr}}} \cdot \left(P^{-3} \dot{P} \right)^{1/2}, \quad (12)$$

where the pulsar period and its derivative are taken in seconds and sec/sec, respectively. The correction parameter L_{corr} was taken to be distributed normally with zero average and standard deviation $\sigma[L_{\text{corr}}] = 0.8$ according to FK06. The constant L_0 (mJy kpc²) is the last free parameter of our simulations and was assumed to be constant and the same for all pulsars during a run.

Synthetic radio flux was then defined as

$$F_{1.4\text{GHz}} = \frac{L_{1.4\text{GHz}}}{d^2}, \quad (13)$$

where d is the modelled distance to the pulsar from the Solar System Barycenter in kiloparsecs.

^c Conventional pseudo-luminosity allows to predict the observed radio flux of a pulsar in a statistical sense rather reflects its real radio luminosity.

Death line

The pulsar death line was adopted in the form

$$\dot{P}_{\text{crit}} = (2.82 \cdot 10^{-17} \text{ sec}^2) P^3 \quad (14)$$

which was initially established by Rawley, Taylor, and Davis 1986 from the observations of a long-period pulsar. This death line is equivalent to the equation used by FK06 ($B/P^2 < 0.17 \times 10^{12} \text{ Gs/sec}^2$) if one assumes $B = 3.2 \cdot 10^{19} \sqrt{PP} \text{ Gs}$ – the standard estimation of pulsar magnetic field. Being a purely empirical filter, equation (14) is still close to the classical theoretical prediction $\dot{P}_{\text{crit}} \propto P^{2.25}$ by Ruderman and Sutherland 1975.

3.5 Pulsar observational selection

Viewing geometry

We assume that synthetic pulsars emit within two identical symmetric pencil-shape beams directed along the magnetic axis. The radius ρ of each beam was calculated according to Rankin's formula for the opening angle of pulsar outer conal emission

$$\rho = 5.7^\circ P^{-1/2}, \quad (15)$$

where P is in seconds (J. M. Rankin 1993a).

The unscattered pulse width w_{10} (at a tenth of maximum) has been then calculated for every synthetic pulsar. Geometrically, it follows the equation

$$\cos \left(\frac{w_{10}}{2} \right) = C(\alpha, \rho, \theta) = \frac{\cos \rho - \cos \alpha \cos \theta}{\sin \alpha \sin \theta}, \quad (16)$$

where $\theta \in 0..180^\circ$ is the observer's obliquity relative to the NS spin axis: $\cos \theta = -(\mathbf{w} \cdot \mathbf{d})$. The pulse width (16) has been calculated for both pulsar beams so that $C_n = C(\alpha, \rho, \theta)$ for "north" beam and $C_s = C(180^\circ - \alpha, \rho, \theta)$ for the "south" one respectively.

The decision about whether the simulated pulsar is "directed" to the observer at the moment of its age t was made as follows:

- If $|C_n| < 1$ then pulsar is detectable and $w_{10} = 2 \arccos(C_n)$ independently on the value C_s ;
- If $|C_n| > 1$ and $|C_s| < 1$ then pulsar is detectable and $w_{10} = 2 \arccos(C_s)$;
- If $|C_n| > 1$ and $|C_s| > 1$ then pulsar can no be detected.

Detection threshold and control subset

We almost replicated the algorithm described in FK06 to model the telescope sensitivity. In particular, we aim to reproduce pulsars detectable by the Parkes and Swinburne Multibeam Surveys (Manchester et al. 2001; Edwards et al. 2001). There are 1057 isolated, rotation-powered pulsars found in the ATNF database, detected within these surveys at the central frequency of 1.4 GHz. Note, however, that W_{10} values are known only for 381 of them, while full proper motion (v_t) for only 106.

To estimate survey sensitivity, the background brightness temperature T_{sky} is needed. We calculated it in a slightly different way than the one used by FK06. Specifically, while

Table 1. Population synthesis best parameters

Parameter	Value
Average initial period $\langle P_0 \rangle$	0.3 sec
Initial period dispersion $\sigma[P_0]$	0.2 sec
Average magnetic field $\langle \log(B/\text{Gs}) \rangle$	12.45
Magnetic field dispersion $\sigma[\log(B/\text{Gs})]$	0.6
Luminosity constant L_0	$4.27 \cdot 10^6$ mJy kpc ²
Derived parameters: isotropic kick	
Pulsar average lifetime	2.4 Myr
Potentially detectable pulsars in Galaxy	62,000
Pulsar average birthrate	2.9 ± 0.1 century ⁻¹
Derived parameters: correlated kick	
Pulsar average lifetime	3.0 Myr
Potentially detectable pulsars in Galaxy	74,000
Pulsar average birthrate	2.8 ± 0.1 century ⁻¹

FK06 have used an electronic version of the T_{sky} maps obtained by Haslam *et al.* 1981 at the central frequency 408 MHz, in our work, we adopted the analytical approximation of the same maps found by Narayan 1987 in the form

$$T_{\text{sky}}(@408\text{MHz}) = 25 + \frac{275}{[1 + (l/42)^2] \cdot [1 + (b/3)^2]} \text{ K}, \quad (17)$$

where l and b are galactic longitude and latitude, respectively, taken in degrees. After that, T_{sky} was scaled to 1.4 GHz according to a power law with $\alpha_{\text{bg}} = -2.8$ spectral slope (Lawson *et al.* 1987). The brightness temperature T_{sky} at the sky coordinates of a synthetic pulsar, as well as the dispersion measure DM towards its position^d were then used to estimate interstellar distortion of the signal and survey detection threshold $F_{1.4, \text{min}} \propto T_{\text{sky}} \sqrt{DM}$. Observed pulse width W_{10} also took into account the interstellar dispersion and telescope parameters.

4. Results

4.1 Pulsar population in general

We have considered a discrete grid in the space of free parameters of our model. There are five of them: two for describing the initial period's distribution ($\langle P_0 \rangle$ and $\sigma[P_0]$), two for magnetic fields ($\langle \log B \rangle$ and $\sigma[\log B]$), and a constant L_0 for a luminosity-period relationship. The grid steps were chosen equal to 0.05 dex for the initial spin period and magnetic field distribution parameters and 0.125 dex for the luminosity normalization constant L_0 . Their values that correspond to the best similarity of synthetic and observed distributions are listed in Table 1. The amount of potentially detectable galactic pulsars and their estimated birthrate are also provided.

These parameters are consistent with those obtained in FK06 and more recent analysis by Igoshev *et al.* 2022. Interestingly, our model predicts not long lifetimes of pulsars: 2.5–3

d. Which was calculated using the galactic electron density model by Cordes and Lazio 2002 to be consistent with the initial FK06 setup.

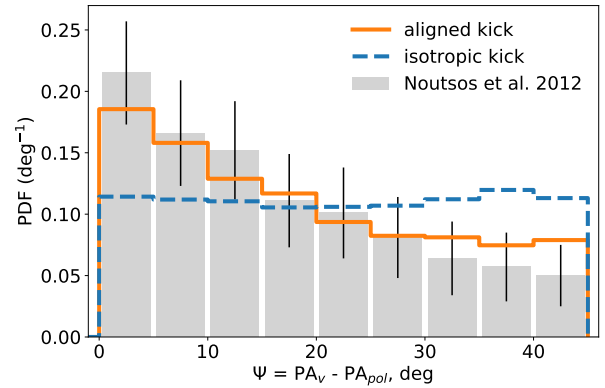


Figure 3. Distributions of the angle $\Psi = PA_v - PA_{pol}$, representing the divergence between the proper motion vector and the pulsar spin axis projection onto the viewing plane. The grey bars display the observed distribution, taken from Noutsos *et al.* 2012, and based on 54 pulsars. Values are normalized from 0 to 45 degrees due to the Rotating Vector Model's degeneracy regarding the X- and O- orthogonal polarisation modes in pulsar emission. Angle Ψ is the only parameter sensitive to the spin-velocity correlation. An isotropic kick scenario (shown by the blue dashed line) results in a nearly uniform distribution of Ψ , inconsistent with observations. On the other hand, a spin-aligned kick scenario (the solid orange line) creates a more suitable, non-uniform distribution.

Myr on average, although much older pulsars are undoubtedly possible. But, within this time interval, one could expect that the peculiar velocity of a pulsar still reflects its natal kick velocity. This makes possible the distribution split found in Figure 2.

The corresponding synthetic distributions of pulsar observables are shown in Figure 6 of the Appendix 1. The solid orange and dashed blue lines are for the aligned and isotropic kick scenarios. The gray-filled histograms show observed distributions (for 1057 control objects). Following Faucher-Giguère and Kaspi 2006, we plot classical magnetic field estimation instead of spin period derivative:

$$B_{\text{md}} = 3.2 \cdot 10^{19} \sqrt{P\dot{P}} \text{ Gs}, \quad (18)$$

where P and \dot{P} are taken in seconds and sec/sec respectively^e. We conclude that the obtained synthetic distributions are close to the observed ones.

Additionally, in Figure 7 of Appendix 1, we show the distributions of more pulsar parameters, which are important for analyzing their kinematics and viewing geometry. They are the magnetic angle α , pulse width at the 10 per cent of maxima (W_{10}), proper motion components $\mu_l \cos b$ and μ_b , transverse velocity v_t and distance d .

These parameters do not so well reproduce the observed distributions. However, this is not unexpected since we ignored any selectional bias that could affect estimations of pulsar

e. Notice, that coefficient $3.2 \cdot 10^{19}$ Gs in equation (18) is formally calculated for a 10km NS with $I = 10^{45}$ g cm² assuming simple magnetodipolar spin-down and $\alpha = 90^\circ$. Therefore, B_{md} is a quantity substituting the \dot{P} rather than a robust estimation of a pulsar magnetic field. See also Biryukov, Astashenok, and Beskin 2017 for additional discussion.

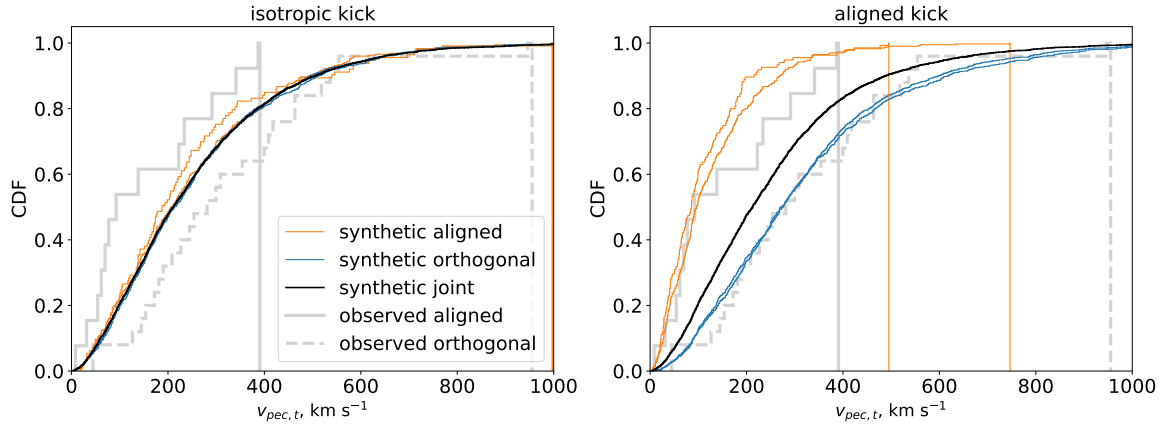


Figure 4. These plots represent the main theoretical result of the paper. Here the distributions of pulsar modelled (synthetic) peculiar velocities $v_{\text{pec}} = \mathbf{v} - \mathbf{v}_{\text{LSR}}$ are shown after their projection onto the viewing plane. The top plot contains results for spin-aligned kick velocity, while the bottom is for isotropic one. The solid black lines show overall pulsar velocity distributions. Observational selection effects, however, are taken into account in the same way as for distributions shown in Figures 6 and 7. The thin orange and blue lines on both plots represent velocity distributions for nearly aligned (with $\alpha < 25$ and 10 degrees) and nearly orthogonal (with $\alpha > 65$ and 80 degrees) pulsars, respectively. The clear effect seen in simulated data is the splitting of the velocity distribution for these two types of pulsars in the case of spin-kick alignment. Specifically, weakly oblique pulsars have systematically smaller and less dispersed observed transverse velocities than orthogonal ones. At the same time, the isotropy of the kick destroys this effect. The observed distributions from Figure 2 are also shown on the plots by light grey lines. Notably, observed and synthetic distributions are very close to each other in the case of spin-kick alignment, although it was not a goal of the calculations. Generally, this plot shows that in a synthetic galaxy of pulsars with realistic underline properties, spin-kick alignment will manifest itself in different transverse velocities of aligned and orthogonal pulsars. Moreover, the strength of such a difference is very close to that observed.

proper motions and distances (and, therefore, transverse velocities). In our model, synthetic pulsars have systematically larger observed velocities (for approximately 150 km s^{-1}). We assume that there are at least two types of selection effects which can work for this difference. The first is the systematic errors in estimating the velocities of slow pulsars, leading to positive false detection of small v_t . The second one is the small number of pulsars used for verification of kick velocity distribution 8. Thus, in FK06, the subset of only 34 pulsars initially observed by Walter F. Brisken et al. 2002; W. F. Brisken et al. 2003 was used. Ultimately, this slight inconsistency can't affect our results. However, we can conclude that none of these parameters are sensitive to the specific spin-kick alignment scenario.

The only parameter which shows such sensitivity is the angle Ψ between the projections of the pulsar spin and velocity vectors. Its properties have been investigated in detail earlier (Simon Johnston et al. 2005; Noutsos et al. 2012; Noutsos et al. 2013). It shows non-uniform distribution, the primary statistical evidence for the pulsar spin-kick correlation. The orientation of the spin axis on the sky is associated with the position angle PA_{pol} of linear polarization of pulsar emission. In particular, the PA_{pol} is associated with the maximum derivative of PA swing. However, we can't distinguish between clockwise and counter-clockwise rotating pulsars in observations. This leads to a 90 -degree uncertainty in angle Ψ . Also, we can not differentiate between X- and O- modes of pulsar polarization, which makes such uncertainty even stronger. As a result, observable Ψ , in fact, is the smallest angle between the proper motion direction PA_v and one of the two axes: one is given by the position angle PA_{pol} and the other by $PA_{\text{pol}} + 90^\circ$.

Synthetic distributions of Ψ obtained in the population

synthesis and the observed one from Noutsos et al. 2012 are shown in Figure 3. We conclude that isotropic kick can not reproduce the observations, while spin-aligned one has such ability. This result is consistent with one obtained by Noutsos et al. 2012 but based on an extensive detailed population synthesis.

4.2 Velocities of aligned and orthogonal rotators

However, the main parameter we are interested in the current work is the peculiar transverse velocities of the pulsars. In Figure 4, we show the modelled distributions of this quantity – similar to that on the starting Figure 2. Solid black lines show resultant distributions which involve every synthetic pulsar and look almost identical in both scenarios of the spin-kick relationship. But, if one considers weakly and strongly oblique pulsars separately, then a high spin-kick alignment produces a clear split in their distributions. This can be seen on the right plot of the Figure 4. A couple of distributions correspond to nearly aligned synthetic pulsars with α less than either 25 or 10 degrees are shown by thin orange lines. Similar distributions for almost orthogonal objects (with α greater than 65 and 80 degrees) are shown by thin blue lines. These two distribution sets are separated from each other, as well as the joint one. In particular, aligned pulsars show systematically smaller and less scattered transverse velocities. This is precisely what is expected in the case of strong spin-kick alignment and is what we observe in real pulsars. Real distributions from Figure 2 are also shown on these plots by light grey lines.

Notably, the modelled distributions on the top plot agree well with the observed ones. This coincidence was not the goal of the simulations and likely represents the adequacy and realism of the constructed population synthesis model.

Finally, we conclude that the performed population synthesis supports the idea that the observed difference in velocities of aligned and orthogonal pulsars is due to spin-kick correlation. Moreover, the kick velocity tends to be aligned with the spin axis direction.

5. Discussion and conclusions

An alternative scenario – when kick velocity is nearly orthogonal to the spin axis – was not considered in detail in our work. However, we also performed simple Monte Carlo calculations for this scenario to ensure completeness. Thus, we assumed that radiopulsars are rotators with magnetic angles that are strictly equal to 0 or 90 degrees. In other words, two extreme cases were considered: fully aligned and fully orthogonal rotators. We model a velocity vector for each pulsar so that its angle to either spin axes or the star's equatorial plane was normally distributed with a dispersion of 15 degrees. Azimuthal orientation of the velocity was chosen uniformly in the 0..360 degrees range. Velocity absolute values were taken from the Maxwellian distribution with an average of 250 km s^{-1} . Modelling 10^7 such synthetic pulsars, we calculated theoretical distributions of transverse velocities – i.e. velocities projected to a common plane. These distributions are shown in the Figure 5. The case of a spin-aligned kick is shown on the top plot of this figure. The character of the difference between the transverse velocities of strictly aligned and orthogonal pulsars is entirely the same as observed (see Figure 2) and obtained in the population synthesis (see Figure 4).

On the other hand, spin-orthogonal kick produces the inverse difference in these distributions. In particular, magnetically orthogonal pulsars show smaller and less dispersed velocities than magnetically aligned ones. Therefore, we conclude that the observed diversity between the velocities of two types of pulsars indicates alignment but not orthogonality of their spin and 3D velocity direction. This is the first time such evidence has been obtained for a subset of pulsars, but not for individual ones, independently of their polarization.

This work has shown the power of the pulsar velocities analysis method in revealing the spin-kick alignment phenomenon. This effect was initially established after analysing 54 pulsars (Noutsos et al. 2012) more than a decade ago. However, recent massive estimations of pulsar polarization parameters, including magnetic angles for more than 400 southern (S. Johnston et al. 2023) and almost 200 northern (Wang et al. 2023) pulsars open a new possibility to refine underline distributions and provide a more detailed understanding of this phenomenon. At the same time, it is evident that transverse velocities of relatively young orthogonal pulsars are the best estimations of their actual 3D velocities, which can be constrained for the first time. This fact could also be used as a basis for further analysis, which will be presented in future works.

Acknowledgement

The authors are thankful to Sergey Popov and Andrei Igoshev for useful suggestions.

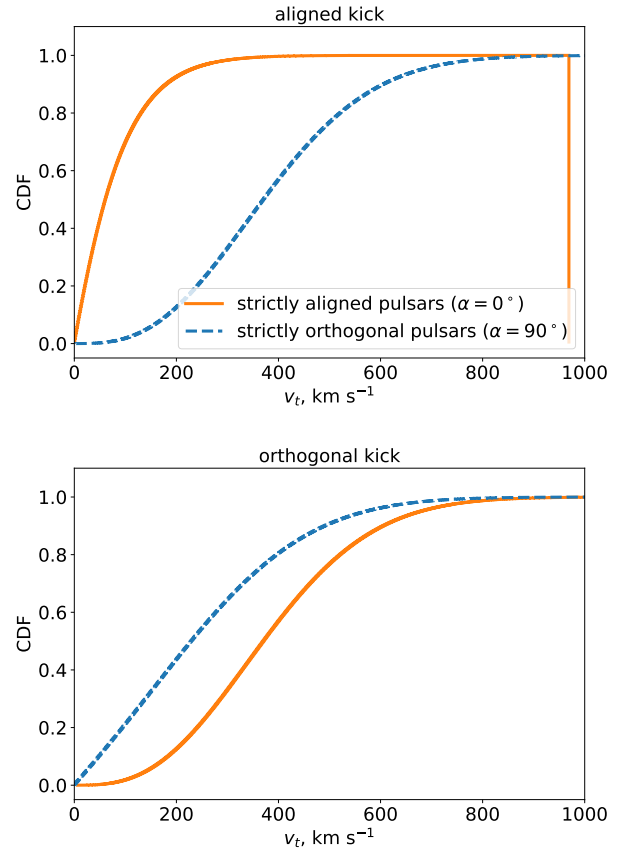


Figure 5. The results of a simple Monte Carlo calculation of pulsar transverse velocities distribution. The top plot represents the case of spin-aligned pulsar velocity in magnetically aligned and orthogonal pulsars. The difference between the distributions is the same as that detected in the observations and found in the population synthesis above. On the other hand, the bottom plot shows a similar distribution but for the case of the kick, which is perpendicular to the spin axis. In this case, the split between two distributions still occurs but has a different sign. In particular, magnetically orthogonal pulsars have qualitatively smaller and less dispersed transverse velocities. This argument supports the conclusion that Figure 2 reflects the spin-kick alignment but not orthogonality. See the text for details.

Funding Statement This work was supported under the Ministry of Science and Higher Education of the Russian Federation grant 075-15-2022-262 (13.MNPMU.21.0003).

Competing Interests None.

Data Availability Statement All the data related to the described analysis can be provided upon request.

References

- Arzoumanian, Z., D. F. Chernoff, and J. M. Cordes. 2002. The Velocity Distribution of Isolated Radio Pulsars. *Astrophys. J* 568, no. 1 (March): 289–301. <https://doi.org/10.1086/338805>. arXiv: astro-ph/0106159 [astro-ph].
- Biryukov, A., A. Astashenok, and G. Beskin. 2017. Refinement of the timing-bases estimator of pulsars magnetic field. *MNRAS* 466:4320–4331. <https://doi.org/10.1093/mnras/stw3341>.

- Biryukov, Anton, and Gregory Beskin. 2023. Imprint of magnetic obliquity in apparent spin-down of radio pulsars. *MNRAS* 522, no. 4 (July): 6258–6263. <https://doi.org/10.1093/mnras/stad1437>. arXiv: 2305.09184 [astro-ph.HE].
- Brisken, W. F., A. S. Fruchter, W. M. Goss, R. M. Herrnstein, and S. E. Thorsett. 2003. Proper-Motion Measurements with the VLA. II. Observations of 28 Pulsars. *Astron. J* 126, no. 6 (December): 3090–3098. <https://doi.org/10.1086/379559>. arXiv: astro-ph/0309215 [astro-ph].
- Brisken, Walter F., John M. Benson, W. M. Goss, and S. E. Thorsett. 2002. Very Long Baseline Array Measurement of Nine Pulsar Parallaxes. *Astrophys. J* 571, no. 2 (June): 906–917. <https://doi.org/10.1086/340098>. arXiv: astro-ph/0204105 [astro-ph].
- Carlberg, R. G., and K. A. Innanen. 1987. Galactic chaos and the circular velocity at the sun. *Astron. J* 94:666–670. <https://doi.org/10.1086/114503>.
- Carretero-Castrillo, M., M. Ribó, and J. M. Paredes. 2023. Galactic runaway O and Be stars found using Gaia DR3. *Astron. and Astrophys.* 679 (November): A109. <https://doi.org/10.1051/0004-6361/202346613>. arXiv: 2311.01827 [astro-ph.SR].
- Chatterjee, S., W. F. Brisken, W. H. T. Vlemmings, W. M. Goss, T. J. W. Lazio, J. M. Cordes, S. E. Thorsett, E. B. Fomalont, A. G. Lyne, and M. Kramer. 2009. Precision Astrometry with the Very Long Baseline Array: Parallaxes and Proper Motions for 14 Pulsars. *Astrophys. J* 698, no. 1 (June): 250–265. <https://doi.org/10.1088/0004-637X/698/1/250>. arXiv: 0901.1436 [astro-ph.SR].
- Coleman, Matthew S. B., and Adam Burrows. 2022. Kicks and induced spins of neutron stars at birth. *MNRAS* 517, no. 3 (December): 3938–3961. <https://doi.org/10.1093/mnras/stac2573>. arXiv: 2209.02711 [astro-ph.HE].
- Cordes, J. M., and David F. Chernoff. 1998. Neutron Star Population Dynamics. II. Three-dimensional Space Velocities of Young Pulsars. *Astrophys. J* 505, no. 1 (September): 315–338. <https://doi.org/10.1086/306138>. arXiv: astro-ph/9707308 [astro-ph].
- Cordes, J. M., and T. J. W. Lazio. 2002. NE2001.I. A New Model for the Galactic Distribution of Free Electrons and its Fluctuations. *ArXiv Astrophysics e-prints* (July). astro-ph/0207156.
- Disberg, P., N. Gaspari, and A. J. Levan. 2024. Deceleration of kicked objects due to the Galactic potential. *Astron. and Astrophys.* 687 (July): A272. <https://doi.org/10.1051/0004-6361/202449996>. arXiv: 2405.06436 [astro-ph.GA].
- Edwards, R. T., M. Bailes, W. van Straten, and M. C. Britton. 2001. The Swinburne intermediate-latitude pulsar survey. *MNRAS* 326:358–374. <https://doi.org/10.1046/j.1365-8711.2001.04637.x>. eprint: astro-ph/0105126.
- Edwards, R. T., G. B. Hobbs, and R. N. Manchester. 2006. TEMPO2, a new pulsar timing package – II. The timing model and precision estimates. *MNRAS* 372, no. 4 (November): 1549–1574. <https://doi.org/10.1111/j.1365-2966.2006.10870.x>. arXiv: astro-ph/0607664 [astro-ph].
- Faucher-Giguère, C.-A., and V. M. Kaspi. 2006. Birth and Evolution of Isolated Radio Pulsars. *Astrophys. J* 643:332–355. <https://doi.org/10.1086/501516>. eprint: astro-ph/0512585.
- Gangadhara, R. T. 1997. Orthogonal polarization mode phenomenon in pulsars. *Astron. and Astrophys.* 327 (November): 155–166. <https://doi.org/10.48550/arXiv.astro-ph/9707168>. arXiv: astro-ph/9707168 [astro-ph].
- Georgelin, Y. M., and Y. P. Georgelin. 1976. The spiral structure of our Galaxy determined from H II regions. *Astron. and Astrophys.* 49:57–79.
- Gullón, M., J. A. Miralles, D. Viganò, and J. A. Pons. 2014. Population synthesis of isolated neutron stars with magneto-rotational evolution. *MNRAS* 443:1891–1899. <https://doi.org/10.1093/mnras/stu1253>. arXiv: 1406.6794 [astro-ph.HE].
- Haslam, C. G. T., U. Klein, C. J. Salter, H. Stoffel, W. E. Wilson, M. N. Cleary, D. J. Cooke, and P. Thomasson. 1981. A 408 MHz all-sky continuum survey. I – Observations at southern declinations and for the North Polar region. *Astron. and Astrophys.* 100:209–219.
- Hobbs, G., D. R. Lorimer, A. G. Lyne, and M. Kramer. 2005. A statistical study of 233 pulsar proper motions. *MNRAS* 360, no. 3 (July): 974–992. <https://doi.org/10.1111/j.1365-2966.2005.09087.x>. arXiv: astro-ph/0504584 [astro-ph].
- Igoshev, Andrei P. 2020. The observed velocity distribution of young pulsars – II. Analysis of complete PSRπ. *MNRAS* 494, no. 3 (May): 3663–3674. <https://doi.org/10.1093/mnras/staa958>. arXiv: 2002.01367 [astro-ph.HE].
- Igoshev, Andrei P., Anastasia Frantsuzova, Konstantinos N. Gourgouliatos, Savina Tschli, Lydia Konstantinou, and Sergei B. Popov. 2022. Initial periods and magnetic fields of neutron stars. *MNRAS* 514, no. 3 (August): 4606–4619. <https://doi.org/10.1093/mnras/stac1648>. arXiv: 2205.06823 [astro-ph.HE].
- Janka, Hans-Thomas. 2017. Neutron Star Kicks by the Gravitational Tugboat Mechanism in Asymmetric Supernova Explosions: Progenitor and Explosion Dependence. *Astrophys. J* 837, no. 1 (March): 84. <https://doi.org/10.3847/1538-4357/aa618e>. arXiv: 1611.07562 [astro-ph.HE].
- Janka, Hans-Thomas, Annap Wongwathanarat, and Michael Kramer. 2022. Supernova fallback as Origin of Neutron Star Spins and Spin-kick Alignment. *Astrophys. J* 926, no. 1 (February): 9. <https://doi.org/10.3847/1538-4357/ac403c>. arXiv: 2104.07493 [astro-ph.HE].
- Johnston, S., M. Kramer, A. Karastergiou, M. J. Keith, L. S. Oswald, A. Parthasarathy, and P. Weltevrede. 2023. The Thousand-Pulsar-Array programme on MeerKAT – XI. Application of the rotating vector model. *MNRAS* 520, no. 4 (April): 4801–4814. <https://doi.org/10.1093/mnras/stac3636>. arXiv: 2212.03988 [astro-ph.HE].
- Johnston, Simon, G. Hobbs, S. Vigeland, M. Kramer, J. M. Weisberg, and A. G. Lyne. 2005. Evidence for alignment of the rotation and velocity vectors in pulsars. *MNRAS* 364, no. 4 (December): 1397–1412. <https://doi.org/10.1111/j.1365-2966.2005.09669.x>. arXiv: astro-ph/0510260 [astro-ph].
- Johnston, Simon, and Michael Kramer. 2019. On the beam properties of radio pulsars with interpulse emission. *MNRAS* 490, no. 4 (December): 4565–4574. <https://doi.org/10.1093/mnras/stz2865>. arXiv: 1910.04550 [astro-ph.HE].
- Keith, M. J., S. Johnston, P. Weltevrede, and M. Kramer. 2010. Polarization measurements of five pulsars with interpulses. *MNRAS* 402, no. 2 (February): 745–752. <https://doi.org/10.1111/j.1365-2966.2009.15926.x>. arXiv: 0910.4778 [astro-ph.SR].
- Kuijken, K., and G. Gilmore. 1989. The mass distribution in the galactic disc. I – A technique to determine the integral surface mass density of the disc near the sun. *MNRAS* 239:571–603. <https://doi.org/10.1093/mnras/239.2.571>.
- Lawson, K. D., C. J. Mayer, J. L. Osborne, and M. L. Parkinson. 1987. Variations in the Spectral Index of the Galactic Radio Continuum Emission in the Northern Hemisphere. *MNRAS* 225:307. <https://doi.org/10.1093/mnras/225.2.307>.
- Lyne, A. G., and R. N. Manchester. 1988. The shape of pulsar radio beams. *MNRAS* 234:477–508. <https://doi.org/10.1093/mnras/234.3.477>.
- Lyutikov, Maxim. 2016. Relativistic Rotating Vector Model. *ArXiv e-prints* (July): arXiv:1607.00777. <https://doi.org/10.48550/arXiv.1607.00777>. arXiv: 1607.00777 [astro-ph.HE].
- Maciesiak, Krzysztof, Janusz Gil, and Valério A. R. M. Ribeiro. 2011. On the pulse-width statistics in radio pulsars – I. Importance of the interpulse emission. *MNRAS* 414, no. 2 (June): 1314–1328. <https://doi.org/10.1111/j.1365-2966.2011.18471.x>. arXiv: 1102.3348 [astro-ph.GA].

- Malov, I. F., and E. B. Nikitina. 2013. The magnetospheric structure of radio pulsars with interpulses. *Astronomy Reports* 57 (November): 833–843. <https://doi.org/10.1134/S106377291311005X>.
- Manchester, R. N., G. B. Hobbs, A. Teoh, and M. Hobbs. 2005. The Australia Telescope National Facility Pulsar Catalogue. *AJ* 129:1993–2006. <https://doi.org/10.1086/428488>. eprint: astro-ph/0412641.
- Manchester, R. N., A. G. Lyne, F. Camilo, J. F. Bell, V. M. Kaspi, N. D’Amico, N. P. F. McKay, et al. 2001. The Parkes multi-beam pulsar survey – I. Observing and data analysis systems, discovery and timing of 100 pulsars. *MNRAS* 328:17–35. <https://doi.org/10.1046/j.1365-8711.2001.04751.x>. eprint: astro-ph/0106522.
- Mandel, Ilya, and Andrei P. Igoshev. 2023. The Impact of Spin-kick Alignment on the Inferred Velocity Distribution of Isolated Pulsars. *Astrophys. J* 944, no. 2 (February): 153. <https://doi.org/10.3847/1538-4357/acb3c3>. arXiv: 2210.12305 [astro-ph.HE].
- Narayan, R. 1987. The birthrate and initial spin period of single radio pulsars. *Astrophys. J.* 319:162–179. <https://doi.org/10.1086/165442>.
- Noutsos, A., M. Kramer, P. Carr, and S. Johnston. 2012. Pulsar spin-velocity alignment: further results and discussion. *MNRAS* 423, no. 3 (July): 2736–2752. <https://doi.org/10.1111/j.1365-2966.2012.21083.x>. arXiv: 1205.2305 [astro-ph.GA].
- Noutsos, A., D. H. F. M. Schnitzeler, E. F. Keane, M. Kramer, and S. Johnston. 2013. Pulsar spin-velocity alignment: kinematic ages, birth periods and braking indices. *MNRAS* 430:2281–2301. <https://doi.org/10.1093/mnras/stt047>. arXiv: 1301.1265.
- Philippov, A., A. Tchekhovskoy, and J. G. Li. 2014. Time evolution of pulsar obliquity angle from 3D simulations of magnetospheres. *MNRAS* 441:1879–1887. <https://doi.org/10.1093/mnras/stu591>. arXiv: 1311.1513 [astro-ph.HE].
- Radhakrishnan, V., and D. J. Cooke. 1969. Magnetic Poles and the Polarization Structure of Pulsar Radiation. *Astrophys. J. Lett.* 3 (January): 225.
- Rankin, J. M. 1993a. Toward an empirical theory of pulsar emission. VI – The geometry of the conal emission region. *Astrophys. J.* 405:285–297. <https://doi.org/10.1086/172361>.
- . 1993b. Toward an empirical theory of pulsar emission. VI – The geometry of the conal emission region: Appendix and tables. *Astrophys. J. Suppl.* 85:145–161. <https://doi.org/10.1086/191758>.
- Rankin, Joanna M. 1990. Toward an Empirical Theory of Pulsar Emission. IV. Geometry of the Core Emission Region. *Astrophys. J* 352 (March): 247. <https://doi.org/10.1086/168530>.
- Rawley, L. A., J. H. Taylor, and M. M. Davis. 1986. Period derivative and orbital eccentricity of binary pulsar 1953 + 29. *Nature* 319:383. <https://doi.org/10.1038/319383a0>.
- Ruderman, M. A., and P. G. Sutherland. 1975. Theory of pulsars – Polar caps, sparks, and coherent microwave radiation. *Astrophys. J.* 196:51–72. <https://doi.org/10.1086/153393>.
- Schönrich, Ralph, James Binney, and Walter Dehnen. 2010. Local kinematics and the local standard of rest. *MNRAS* 403, no. 4 (April): 1829–1833. <https://doi.org/10.1111/j.1365-2966.2010.16253.x>. arXiv: 0912.3693 [astro-ph.GA].
- Spitkovsky, A. 2006. Time-dependent Force-free Pulsar Magnetospheres: Axisymmetric and Oblique Rotators. *Astrophys. J. Lett.* 648:L51–L54. <https://doi.org/10.1086/507518>. eprint: astro-ph/0603147.
- Stinebring, D. R., J. M. Cordes, J. M. Rankin, J. M. Weisberg, and V. Boriakoff. 1984. Pulsar polarization fluctuations. I. 1404 MHz statistical summaries. *Astrophys. J. Suppl.* 55 (June): 247–277. <https://doi.org/10.1086/190954>.
- Tetzlaff, N., R. Neuhauser, and M. M. Hohle. 2011. A catalogue of young runaway Hipparcos stars within 3 kpc from the Sun. *MNRAS* 410, no. 1 (January): 190–200. <https://doi.org/10.1111/j.1365-2966.2010.17434.x>. arXiv: 1007.4883 [astro-ph.GA].
- Verbunt, Frank, Andrei Igoshev, and Eric Cator. 2017. The observed velocity distribution of young pulsars. *Astron. and Astrophys.* 608 (December): A57. <https://doi.org/10.1051/0004-6361/201731518>. arXiv: 1708.08281 [astro-ph.HE].
- Wainscoat, R. J., M. Cohen, K. Volk, H. J. Walker, and D. E. Schwartz. 1992. A model of the 8–25 micron point source infrared sky. *Astrophys. J. Suppl.* 83:111–146. <https://doi.org/10.1086/191733>.
- Wang, Chen, Dong Lai, and J. L. Han. 2006. Neutron Star Kicks in Isolated and Binary Pulsars: Observational Constraints and Implications for Kick Mechanisms. *Astrophys. J* 639, no. 2 (March): 1007–1017. <https://doi.org/10.1086/499397>. arXiv: astro-ph/0509484 [astro-ph].
- . 2007. Spin-Kick Correlation in Neutron Stars: Alignment Conditions and Implications. *Astrophys. J* 656, no. 1 (February): 399–407. <https://doi.org/10.1086/510352>. arXiv: astro-ph/0607666 [astro-ph].
- Wang, P. F., J. L. Han, J. Xu, C. Wang, Y. Yan, W. C. Jing, W. Q. Su, D. J. Zhou, and T. Wang. 2023. FAST Pulsar Database. I. Polarization Profiles of 682 Pulsars. *Research in Astronomy and Astrophysics* 23, no. 10 (October): 104002. <https://doi.org/10.1088/1674-4527/acea1f>. arXiv: 2307.10340 [astro-ph.HE].
- Wang, P. F., C. Wang, and J. L. Han. 2014. Polarized curvature radiation in pulsar magnetosphere. *MNRAS* 441, no. 3 (July): 1943–1953. <https://doi.org/10.1093/mnras/stu690>. arXiv: 1404.1431 [astro-ph.HE].
- Wiringa, R. B., V. Fiks, and A. Fabrocini. 1988. Equation of state for dense nucleon matter. *Phys. Rev. C* 38:1010–1037. <https://doi.org/10.1103/PhysRevC.38.1010>.
- Yao, Jumei, Weiwei Zhu, Richard N. Manchester, William A. Coles, Di Li, Na Wang, Michael Kramer, et al. 2021. Evidence for three-dimensional spin-velocity alignment in a pulsar. *Nature Astronomy* 5 (May): 788–795. <https://doi.org/10.1038/s41550-021-01360-w>. arXiv: 2103.01839 [astro-ph.GA].
- Yusifov, I., and I. Küçük. 2004. Revisiting the radial distribution of pulsars in the Galaxy. *Astron. and Astrophys.* 422:545–553. <https://doi.org/10.1051/0004-6361:20040152>. eprint: astro-ph/0405559.

Appendix 1. Analyzed pulsar subset details and expanded results of the population synthesis

Table 2. Pulsars under consideration. These classical isolated pulsars are assumed to be either weakly or strongly inclined in terms of their magnetic angle. At the same time, they all have distance estimates and full proper motions. The ages here are characteristic ages $P/2\dot{P}$ in 10^6 years, while the surface fields are magnetodipolar estimates of $3.2 \times 10^{19} \sqrt{P\dot{P}}$ in 10^{12} Gs. The last column lists the references where a particular pulsar has been found to be either aligned or orthogonal.

N	PSR	P , sec	Age, Myr	B_{12} , Gs	Distance, kpc	v_t , km s $^{-1}$	$v_{pec,t}$, km s $^{-1}$	Type	References
1	J0152-1637	0.833	10.17	1.05	2.00 (PX) ^a	206	209	orthogonal	[1], [3] ^b
2	J0406+6138	0.595	1.69	1.84	4.55 (PX)	558	561	orthogonal	[3]
3	J0525+1115	0.354	76.44	0.16	1.84 (DM)	267	262	orthogonal	[2]
4	J0534+2200	0.033	0.00	3.79	2.00 (DM)	143	152	orthogonal	[2], [4]
5	J0820-1350	1.238	9.31	1.64	1.96 (PX)	437	464	orthogonal	[1]
6	J0826+2637	0.531	4.93	0.96	0.50 (PX)	235	232	orthogonal	[1], [2], [4]
7	J0835-4510	0.089	0.01	3.38	0.29 (PX)	62	45	orthogonal	[1], [2]
8	J0908-4913	0.107	0.11	1.28	1.00 (DM)	193	156	orthogonal	[2], [4], [5], [6], [7]
9	J1057-5226	0.197	0.54	1.09	0.09 (DM)	34	52	orthogonal	[1], [2], [4], [5]
10	J1509+5531	0.740	2.35	1.95	2.13 (PX)	964	955	orthogonal	[1]
11	J1645-0317	0.388	3.46	0.84	3.85 (PX)	374	402	orthogonal	[1], [2]
12	J1705-1906	0.299	1.15	1.13	0.75 (DM)	314	306	orthogonal	[1], [2], [4], [6]
13	J1722-3207	0.477	11.74	0.56	2.93 (DM)	541	524	orthogonal	[1]
14	J1731-4744	0.830	0.08	11.81	0.70 (DM)	485	470	orthogonal	[1]
15	J1751-4657	0.742	9.06	0.99	0.74 (DM)	193	176	orthogonal	[1]
16	J1820-0427	0.598	1.50	1.97	2.86 (PX)	262	290	orthogonal	[2]
17	J1841+0912	0.381	5.55	0.65	1.66 (DM)	337	361	orthogonal	[1], [3]
18	J1903+0135	0.729	2.87	1.73	3.30 (DM)	167	133	orthogonal	[1]
19	J1909+0007	1.017	2.92	2.40	4.36 (DM)	602	539	orthogonal	[2], [3]
20	J1909+1102	0.284	1.71	0.88	4.80 (DM)	243	314	orthogonal	[1]
21	J1913-0440	0.826	3.22	1.86	4.04 (DM)	167	191	orthogonal	[1]
22	J1917+1353	0.195	0.43	1.20	5.88 (PX)	260	413	orthogonal	[2]
23	J1919+0021	1.272	2.63	3.16	5.88 (PX)	345	425	orthogonal	[1], [2]
24	J2022+2854	0.343	2.88	0.82	2.70 (PX)	246	187	orthogonal	[1], [2]
25	J2330-2005	1.644	5.63	2.79	0.86 (DM)	262	249	orthogonal	[2]
1	J0157+6212	2.352	0.20	21.33	1.79 (PX)	384	391	aligned	[2]
2	J0502+4654	0.639	1.82	1.91	1.32 (DM)	80	96	aligned	[1], [3]
3	J0659+1414	0.385	0.11	4.65	0.29 (PX)	65	73	aligned	[1]
4	J0946+0951	1.098	4.99	1.98	0.89 (DM)	163	141	aligned	[1]
5	J0953+0755	0.253	17.46	0.24	0.26 (PX)	39	55	aligned	[1], [4], [6]
6	J1302-6350	0.048	0.33	0.33	2.63 (PX)	14	63	aligned	[4]
7	J1543+0929	0.748	27.50	0.58	7.69 (PX)	269	293	aligned	[1], [2]
8	J1720-0212	0.478	91.58	0.20	2.36 (DM)	259	238	aligned	[1]
9	J1946+1805	0.441	290.20	0.10	0.30 (DM)	6	8	aligned	[4], [6]
10	J2006-0807	0.581	200.44	0.17	2.63 (PX)	114	80	aligned	[1], [3]
11	J2113+4644	1.015	22.53	0.86	2.17 (PX)	181	226	aligned	[1], [2]
12	J2149+6329	0.380	35.92	0.26	2.78 (PX)	299	343	aligned	[1]
13	J2325+6316	1.436	8.06	2.04	4.86 (DM)	83	33	aligned	[1]

a DM is for dispersion measure-based distances according to Galactic free electrons distribution by [REF]; PX for the parallax-based distances.

b References that support the type of the obliquity: [1] Lyne and Manchester 1988; [2] Joanna M. Rankin 1990; [3] J. M. Rankin 1993b; [4] Maciesiak, Gil, and Ribeiro 2011; [5] Keith et al. 2010; [6] Malov and Nikitina 2013; [7] Johnston and Kramer 2019.

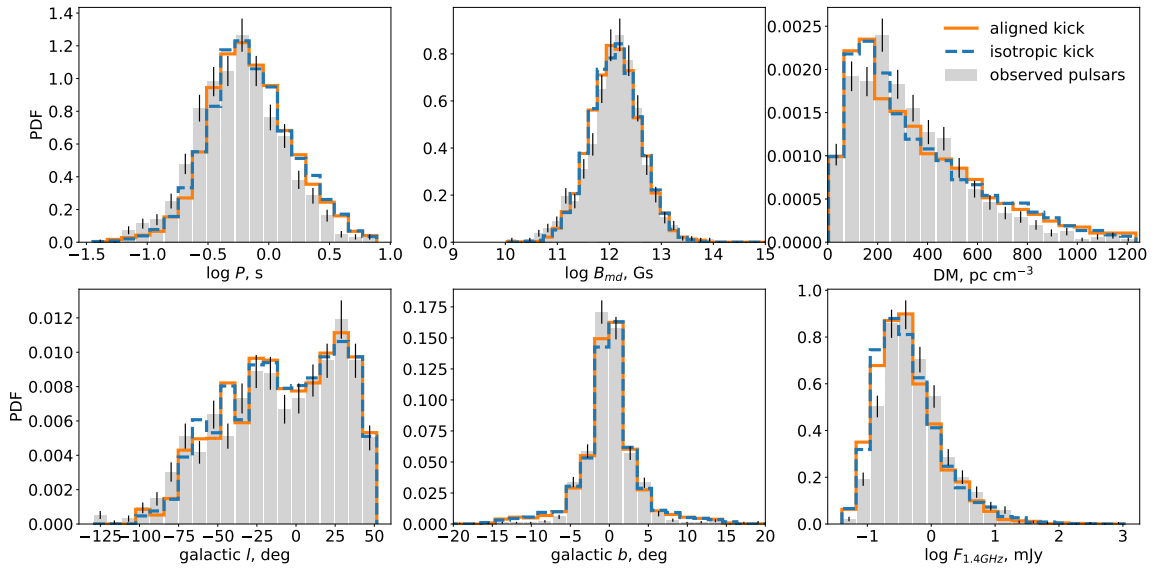


Figure 6. Pulsar population synthesis results show distributions of six observables used to find optimal model parameters: pulsar spin period P , magnetic field $B_{md} \propto \sqrt{P\dot{P}}$, dispersion measure DM , galactic coordinates (l , b), and flux F at 1.4 GHz. The solid orange line shows synthetic distributions assuming a kick velocity aligned with the spin axis, while the dashed blue line represents an isotropic kick. Both models use the same initial parameters from Table 1. Observed distributions for 1057 single classical pulsars from Parkes and Swinburne surveys are shown as grey bars. Population synthesis qualitatively reproduces the observed statistics well, and the plotted quantities are insensitive to the possible spin-kick correlation.

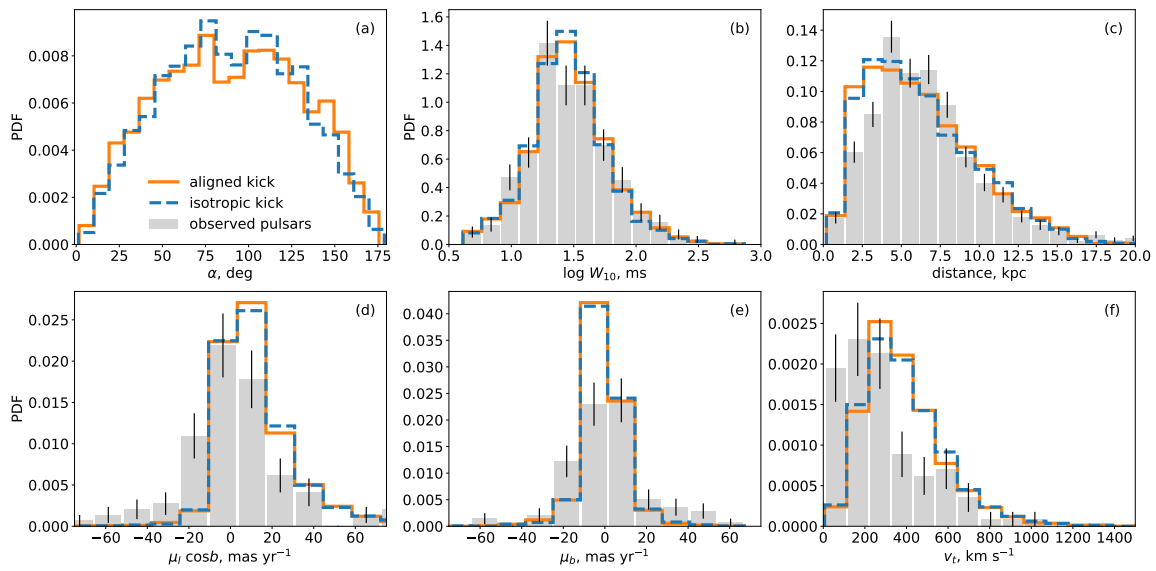


Figure 7. Further results of population synthesis. This figure is organized similarly to the previous one: the grey-shaded bars represent the observed distributions (where applicable), while the orange solid and blue dashed lines are for synthetic distributions. (a) Magnetic angle α between the spin and magnetic angle of synthetic pulsars. Surprisingly, this parameter is insensitive to the specific spin-kick orientation scenario. This is probably due to the nearly anisotropic distribution of pulsars relative to the observer. (b) Pulsar pulse widths at 10% of maximum in milliseconds. The observed distribution is shown for 381 pulsars with measured W_{10} from the control subset of 1057 objects. (c) Distances to pulsars relative to the Solar System barycenter. Observed values are mostly based on the dispersion measure. Here, all 1057 control pulsars are shown. (d) Proper motion along the galactic longitude. The observed distribution is shown for 106 pulsars with known μ_l from the initial control subset. (e) Similar, but for galactic longitudinal direction. (f) Transverse velocities relative to the Solar system barycenter. Relative to this particular control subset of pulsars, the synthetic population shows excess in nearby and faster pulsars. This could be a result of a combination of selection effects in the estimation of pulsar proper motions, systematic errors in estimations of distances as well as some incompleteness of the kick distribution model.